# Meridional Shifts of the Southern Hemisphere Westerlies During the Early Cenozoic

Hongjin Chen[1] ⓘ, Zhaokai Xu[2,3] ⓘ, Germain Bayon[4], Qingchao Fan[2] ⓘ, Philip A. E. Pogge von Strandmann[5], Wei Wang[6], Tianqi Sun[2], and Tiegang Li[7] ⓘ

[1]Key Laboratory of Marine Mineral Resources, Ministry of Natural Resources, Guangzhou Marine Geological Survey, China Geological Survey, Guangzhou, China, [2]Key Laboratory of Ocean Observation and Forecasting, Key Laboratory of Marine Geology and Environment, Institute of Oceanology, Chinese Academy of Sciences, Qingdao, China, [3]Laboratory for Marine Geology, Qingdao Marine Science and Technology Center, Qingdao, China, [4]University Brest, CNRS, Plouzané, France, [5]Institute of Geosciences, Johannes Gutenberg University, Mainz, Germany, [6]State Key Laboratory of Marine Geology, Tongji University, Shanghai, China, [7]Key Laboratory of Marine Sedimentology and Metallogeny, First Institute of Oceanography, Ministry of Natural Resources, Qingdao, China

**Abstract** Despite the crucial role of the Southern Hemisphere (SH) westerlies in modulating modern and past climate evolution, little is known about their behavior and possible forcing mechanisms during the early Cenozoic. We probe changes in the hydroclimate of southwest Australia during 62–51 Ma, based on sedimentary proxy records from the International Ocean Discovery Program Site U1514 in the Mentelle Basin. Our results reveal a transition from a less humid climate to wetter conditions at mid–high latitudes starting from the early Eocene, which suggests poleward migration of the SH westerlies. This long-term trend is punctuated by short-lived events of aridification during the Mid-Paleocene Biotic Event and wetter intervals during the Paleocene-Eocene Thermal Maximum, indicating additional short-term meridional shifting of the westerlies. We propose that the evolution of SH westerlies was driven by the equator-to-pole temperature gradient regulated by global warming and ephemeral growth of the Antarctic ice sheet.

**Plain Language Summary** The Southern Hemisphere (SH) westerlies, which are the dominant atmospheric circulation patterns in the middle latitudes, play a key role in regulating global and regional climate. Currently, the knowledge of past changes in SH westerlies relies mainly on the late Quaternary. Its dynamics over longer timescales, especially under early Cenozoic greenhouse climate states, remain poorly understood. The Mentelle Basin off southwest Australia was located at a more southerly location than at the present day, and was potentially under the influence of SH westerlies. To examine the long-term hydroclimate changes in southwest Australia during the mid-late Paleocene to the early Eocene (62–51 Ma), we measured neodymium and hafnium isotopic compositions of fine-grained detrital sediments from a borehole (IODP Site U1514) drilled in the Mentelle Basin, in addition to clay mineralogy, and elemental abundances. Our results suggest a gradual wetting of southwest Australia since the early Eocene, which we relate to the poleward migration of SH westerlies in response to a reduced latitudinal temperature gradient. An abrupt northward shift of SH westerlies was observed during the short-lived Middle Paleocene Biotic Event (~59 Ma), possibly driven by ephemeral growth of the Antarctica ice sheet.

## 1. Introduction

Characterizing climate dynamics over geological timescales, especially during warm intervals associated with high levels of atmospheric carbon dioxide ($p$CO$_2$), is crucial for understanding the possible future evolution of global climate following ongoing anthropogenic emissions (Komar et al., 2013; Norris et al., 2013; Thomas et al., 2006; Zachos et al., 2008). The Early Cenozoic (~65–34 Ma) stands as a typical greenhouse interval, characterized by high $p$CO$_2$ (1,000–4,000 ppmv), decreased latitudinal temperature gradients, and no/minimal bipolar glaciation (Crame, 2020; Deconto & Pollard, 2003; Pearson & Palmer, 2000; Zachos et al., 2001). The early Cenozoic warmth peaked during the early Eocene (Early Eocene Climatic Optimum, ~53–51 Ma), following a long-term warming trend initiated during the Late Paleocene and Early Eocene (~60–50 Ma) (Kirtland Turner et al., 2014; Westerhold et al., 2020). To date, many studies have focused on short-lived hyperthermal events (e.g., Paleocene-Eocene Thermal Maximum, PETM) that punctuated the Early Cenozoic,

yet the long-term global climate variability and its impact on regional hydroclimate patterns still remain poorly documented (Zachos et al., 2008).

The Southern Hemisphere (SH) westerlies, which are the strongest time-mean surface winds on Earth, play an important role in regulating ocean circulation and in delivering moisture to continental regions located at middle-high latitudes, thus exerting substantial control on continental weathering and erosion, marine biogeochemistry and ocean-atmosphere $CO_2$ exchange (Hodgson & Sime, 2010; Menviel et al., 2018; Saunders et al., 2012). At present, SH westerlies are located within a latitudinal belt of 40–60°S, with their position and intensity varying as a consequence of changes in temperature and pressure gradients between mid-latitudes and Antarctica (Shulmeister et al., 2004). Over millennial timescales, precipitation- or dust-related proxy records and modeling studies consistently indicate a strengthening and poleward migration of the westerlies since the Last Glacial Maximum, possibly corresponding to a smaller interhemispheric temperature contrast under warm climate conditions (Goyal et al., 2021; Lamy et al., 2010). Over longer timescales, however, the dynamics of SH westerlies and their driving mechanisms remain poorly investigated, apart from a few proxy studies mostly focused on the late Cenozoic (Abell et al., 2021; Groeneveld et al., 2017). Reconstructing the response of SH westerlies under different climate states, especially during the warmer-than-present early Cenozoic, is particularly important in order to improve our understanding of the hydroclimate evolution of mid-latitude regions in the context of global warming.

The Mentelle Basin off southwest (SW) Australia, a deep-water sedimentary basin formed during the Paleozoic-Mesozoic breakup of eastern Gondwana, has experienced a complex history of volcanism, rifting activity, and thermal subsidence throughout the Cenozoic (Borissova et al., 2010; Maloney et al., 2011; Sykes & Kidd, 1994). The Mentelle Basin was located in the southern middle–high latitudes (~55°S) during the Early Cenozoic, when southeast Australia was still connected to Antarctica, until the final breakup resulting from the fast-spreading of Southern Ocean during the mid-Eocene (Huber et al., 2019). A much more southerly location than present and significant influence of the SH atmospheric circulation on SW Australia has been suggested at least since the Cretaceous (Groeneveld et al., 2017; Sykes & Kidd, 1994). The well-preserved Cenozoic sediment records in the Mentelle Basin thus provide unique archives for reconstructing the paleoclimate evolution of surrounding continental regions and its link to the SH westerlies (Huber et al., 2019).

In this study, we present a multi-proxy record of clay mineralogy, elemental abundances, and neodymium-hafnium (Nd-Hf) isotopic compositions of the fine-grained siliciclastic fraction of middle-late Paleocene to early Eocene sediments retrieved from International Ocean Discovery Program (IODP) Site U1514. Combined with a well-resolved age model (Huber et al., 2019; Vahlenkamp et al., 2020), this study aims to reconstruct paleoclimatic variations in the source regions at mid–high latitudes and further reveal the evolution of the SH westerlies during the early Cenozoic (~62–51 Ma) (Figure 1).

## 2. Materials and Methods

Site U1514 (33°7.2327′S, 113°5.4672′E) is the northernmost and deepest (water depth: 3,850 m) site drilled in the Mentelle Basin off SW Australia during IODP Expedition 369 (Figure 1; Huber et al., 2019). This study mainly focuses on the interval of 240.7–362.2 m core composite depth below seafloor (CCSF), which spans from the middle–late Paleocene to the early Eocene. The studied section consists of nannofossil chalk with clay, clayey nannofossil chalk, nannofossil-rich claystone and clay stone (Huber et al., 2019). The age model of this section was established by nannofossil and foraminiferal biostratigraphy and magnetostratigraphy, with additional constraints from the chemostratigraphy based on bulk carbonate $\delta^{13}C$ (Table S1 in Supporting Information S1 and Figure S1 in Supporting Information S1) (Edgar et al., 2022; Huber et al., 2019). The stratigraphic location of PETM, characterized by a prominent $\delta^{13}C$ negative excursion, presents at ~280.3 m CCSF of Site U1514 (Edgar et al., 2022; Vahlenkamp et al., 2020).

In this study, a total of 77 samples from Site U1514 were sampled at intervals of ~1.5 m, resulting in a mean temporal resolution of ~0.12 Myr. Detailed descriptions of the analytical methods can be found in the in Supporting Information S1.

## 3. Results

The clay mineral assemblages at Site U1514 are dominated by smectite (70%–98%, average 92%), with illite (1%–20%, average 5%) and kaolinite (0%–16%, average 3%) being present in lesser abundance (Figure S2 in
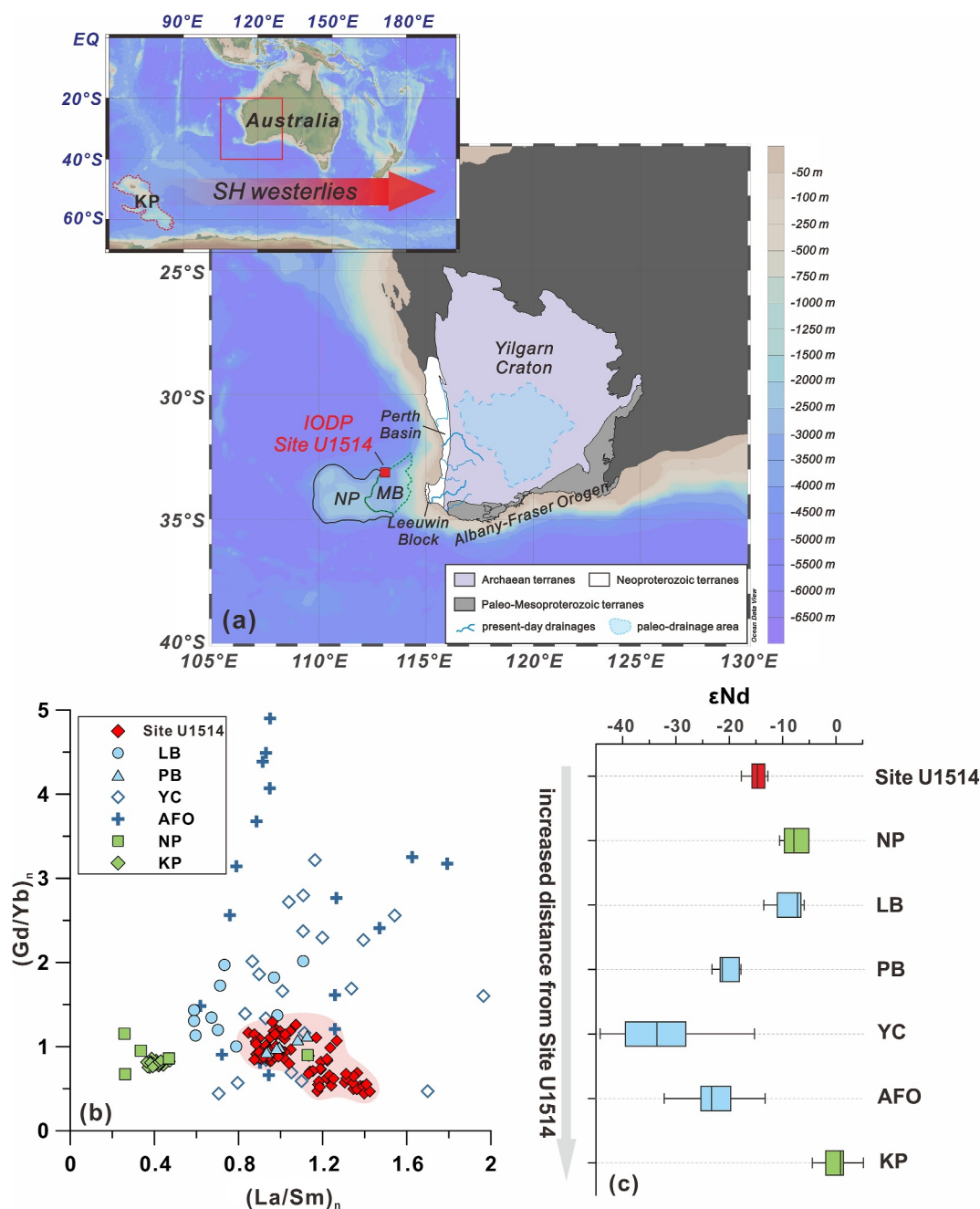
**Figure 1.** (a) Map showing the location of IODP Site U1514 of the Mentelle Basin. Major geological features and drainage systems of SW Australia are indicated (modified after Kohn et al., 2002; Wang et al., 2022). The red arrow shows the present-day SH westerlies. MB = Mentelle Basin, NP = Naturaliste Plateau, KP = Kerguelen Plateau, EQ = equator. (b) Discrimination plot of $(La/Sm)_n$ versus $(Gd/Yb)_n$, and (c) whisker plot of Nd isotope ratios of Site U1514, compared with potential sources (Wang et al., 2022 and references therein). REE values were normalized to Post Archean Australian Shale (PAAS) as indicated by "n", based on Pourmand et al. (2012). LB = Leeuwin Block; PB = Perth Basin; YC = Yilgarn Craton; AFO = Albany-Fraser Orogen; KP = Kerguelen Plateau.

Supporting Information S1 and Dataset S1). Chlorite content is negligible (<1%) throughout the investigated interval. In general, the kaolinite and illite contents show a similar down-core pattern, exhibiting relatively low values during the middle-late Paleocene (62–56 Ma), and followed by an abrupt pulse during the PETM (~55.9 Ma) and a subsequent gradual early Eocene increase (55–51 Ma) (Figure S2 in Supporting Information S1). Variation in the smectite content is inversely related to those of kaolinite and illite. The crystallinity of

smectite varies between 0.59 and 1.83°Δ2θ (average 0.88°Δ2θ), while the illite crystallinity shows a narrow range of values between 0.15 and 0.37 (average 0.25°Δ2θ).

The median grain size of Site U1514 varies between 4.7 and 35.9 μm (average 11.8 μm) (Figure S2 in Supporting Information S1). The MAR$_{siliciclastic}$ ranges from 0.2 to 4.3 g/cm$^2$/kyr, with an average of 0.7 g/cm$^2$/kyr. This index remains relatively steady throughout the studied interval, except for an abrupt peak at ∼59.5 Ma (Figure S2 in Supporting Information S1).

Apart from Mn, elemental abundances of siliciclastic sediment fractions at Site U1514 display similar down-core variability, marked by an upward gradual decrease during the middle-late Paleocene (62–56 Ma) and an upward general increase with large fluctuations during the early Eocene (55–51 Ma), intruded by an abrupt pulse during PETM (Figure S3 in Supporting Information S1). The rare earth elements (REEs) display a similar pattern to those of major elements (Dataset S1).

Nd and Hf isotopic compositions of clay-size siliciclastic fractions at Site U1514 are given in Table S1 in Supporting Information S1. $\varepsilon_{Nd(i)}$ ranges between −17.2 and −12.2 (average −14.2), while $\varepsilon_{Hf(i)}$ varies between −17.9 and −12.7 (average −15.0), plotting between the correlation trends defined by the Clay Array and the Terrestrial Array (Figure S4 in Supporting Information S1). $\varepsilon_{Nd}$ displays limited variability during the middle-late Paleocene (62–56 Ma) and a gradual decreasing trend during the early Eocene (55–51 Ma), whereas $\varepsilon_{Hfclay}$ is punctuated by additional abrupt changes across ∼59.5 Ma and 55.8 Ma (Figure 2).

## 4. Discussion

### 4.1. Sediment Provenance

While source-to-sink processes in the Mentelle Basin have been relatively sparsely investigated compared to the adjacent Perth Basin, recent studies based on sedimentary archives from IODP Expedition 369 have shown that river catchments in SW Australia acted as the main source of sediments to the deep basin, at least since the early Cretaceous (Chen et al., 2022; Fan et al., 2022; Sun et al., 2022; Wang et al., 2022). Three major geological units dominate in SW Australia: Archean gneiss and granitoids (Yilgarn Craton), Paleo-Mesoproterozoic orthogneisses and granitic rocks (i.e., Albany-Fraser Orogen), and Neoproterozoic granitic orthogneisses (i.e., Perth Basin and Leeuwin Block), characterized by distinct geochemical features (Figure 1) (Wilde & Nelson, 2001). Increased sediment contribution from more distal provenance (e.g., Yilgarn Craton) relative to proximal source regions (e.g., Perth Basin and Leeuwin Blocks) has been inferred during short-lived warm intervals such as Oceanic Anoxic Event 2, interpreted as reflecting reactivation of large fluvial systems triggered by an enhanced hydrological cycle (Chen et al., 2022; Wang et al., 2022). Although the final breakup of East Antarctica and southern Australia was incomplete until the late Eocene, detrital supply from East Antarctica was most likely negligible owing to the cessation of the transcontinental fluvial pathway in early Cretaceous (∼136 Ma) (Maritati et al., 2021). In addition, volcanogenic sediments associated with the Kerguelen and Réunion hotspots may have represented substantial sources of terrigenous sediments to the Indian Ocean since the early Cretaceous (Sykes & Kidd, 1994). However, the subsidence and subsequent immergence of the Kerguelen Plateau after 80–70 Ma and the remoteness of the Réunion hotspots from the Mentelle Basin most likely exclude them as dominant sediment sources to the Mentelle Basin (Sykes & Kidd, 1994).

Here, REEs and clay-size radiogenic Nd isotopic ratios are employed as provenance tracers (Bayon et al., 2015). Both REE ratios and $\varepsilon_{Nd}$ indicate that sediments delivered to Site U1514 were mostly sourced from SW Australia and not from distant volcanogenic sources (e.g., Kerguelen Plateau) (Figure 1). Note that igneous rocks from the Naturaliste Plateau, lying at the western flank of the Mentelle Basin, display similar geochemical signatures with sediments as the study site (Figure 1b). Although weathered volcanic products from the southern Naturaliste Plateau have been suggested as a major source of volcaniclastic-rich sequence deposited in the Mentelle Basin during the early Cretaceous breakup of East Gondwana (Lee et al., 2020), the lack of major tectonic events (e.g., rifting and volcanism) and the absence of any volcanic clasts in the investigated sediment interval at Site U1514 indicate no or minor contribution from the Naturaliste Plateau (Huber et al., 2019; White et al., 2022).

In SW Australia, the distal source regions of the Yilgarn Craton and the Albany-Fraser Orogen exhibit highly unradiogenic $\varepsilon_{Nd}$ values (average −33) compared with the proximal geological provinces composing the Leeuwin Block and the Perth Basin (Osei et al., 2021) (Figure 1). The paleo Yilgarn River draining mostly Archean terranes represented a major westward river in SW Australia before the late Eocene drainage reversal
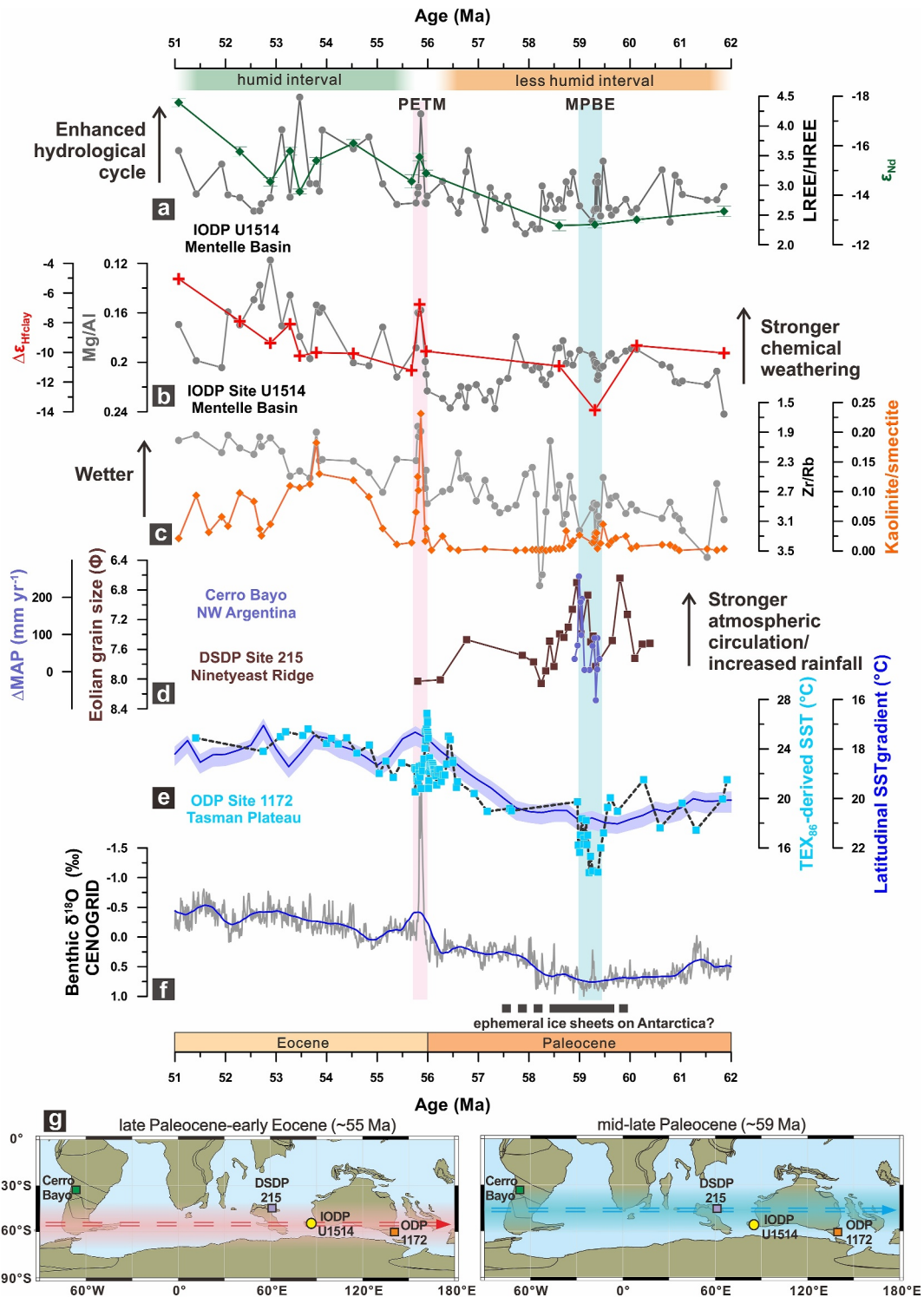
**Figure 2.** Provenance and hydroclimate proxy records at Site U1514 during the Early Cenozoic. (a) $\varepsilon_{Nd}$ and LREE/HREE ratio as provenance indicators, (b) Weathering proxies of $\Delta\varepsilon_{Hfclay}$ and Mg/Al, (c) Humidity proxies of kaolinite/smectite and Zr/Rb ratios at Site U1514, (d) Eolian dust grain size at DSDP Site 215 (Hovan & Rea, 1992) and mean annual precipitation from Paleocene baseline (ΔMAP) of Cerro Bayo (Hyland et al., 2015), (e) SST reconstructed at ODP Site 1,172 (Bijl et al., 2009, 2013; Hollis et al., 2014) and latitudinal SST gradient (Gaskell et al., 2022), (f) Global benthic $\delta^{18}O$ (Westerhold et al., 2020), (g) Schematic maps showing the hypothesized shift in the position of SH westerlies of mid-late Paleocene and late Paleocene-early-Eocene. The paleogeographical reconstruction was generated using ODSN (https://www.odsn.de/odsn/services/paleomap/paleomap.html).

(Beard, 1999) (Figure 1). In contrast, relatively small river systems (e.g., Blackwood River) flowed through the coastal regions of the Perth Basin and the Leeuwin Block), whereas the Albany-Fraser Orogen was mainly drained by southward-flowing rivers (Figure 1). Therefore, the relatively radiogenic $\varepsilon_{Nd}$ signature observed in this study can be largely explained by mixed sediment contribution from the Perth Basin and the Leeuwin Block catchment regions. This inference is also supported by REE discrimination plots, in which samples from Site U1514 show more resemblance to the proximal terranes of SW Australia (Figure 1b).

However, the temporal $\varepsilon_{Nd}$ changes at Site U1514 reveal a small but gradual decreasing trend starting from the early Eocene, consistent with enhanced sediment contribution from distant terranes (Figure 2a). Such change in provenance is further confirmed by the synchronous variation pattern of LREE/HREE ratios at Site U1514, which indicates increased detrital supply from felsic sources (i.e., Yilgran Craton) since the early Eocene (Figure 2a). Large catchments of the Yilgarn River remain almost intermittent or inactive except under climate with exceptionally high rainfall, while small river systems draining the Perth Basin and Leeuwin Block receive comparatively high amounts of precipitation as they lie at the frontal side of the wind belt (Beard, 1999; Chen et al., 2022). Such differences would make sediment discharge from distal catchment regions particularly more sensitive to hydroclimate changes. Therefore, we argue that the siliciclastic sediments of Site U1514 were mainly derived from SW Australia, dominated by contributions from the proximal terranes (i.e., Leeuwin Block and Perth Basin). The provenance remained relatively stable during the early Cenozoic, with a slightly increased contribution from more distal regions in SW Australia starting from the early Eocene, possibly associated with regional climate change (Chen et al., 2022).

## 4.2. Hydroclimate Evolution of SW Australia During the Early Cenozoic

Given that the detrital sediments delivered to Site U1514 were predominately sourced from SW Australia, proxies of climatic parameters (rainfall, temperature) are suitable for reconstructing the paleo-environmental evolution of corresponding source regions. $\Delta\varepsilon_{Hfclay}$, which represents the vertical deviation of $\varepsilon_{Hf}$ from the Clay Array ($\varepsilon_{Hf} = 0.78 \times \varepsilon_{Nd} + 5.23$) defined by the world river clays (Figure S4 in Supporting Information S1), has been successfully applied to trace continental chemical weathering over various geological timescales (Bayon et al., 2022; Chen et al., 2023; Corentin et al., 2022). Enhanced terrestrial weathering is indicated by higher values of $\Delta\varepsilon_{Hfclay}$, resulting from the preferential dissolution of Lu-rich accessory minerals (e.g., phosphate) during incongruent weathering and subsequent release of more radiogenic $\varepsilon_{Hf}$ to surface environments (Bayon et al., 2016). Besides, the intensity of chemical weathering can be also constrained by the ratio of mobile versus immobile elements (e.g., Mg/Al), which has been widely applied in many marine archives (e.g., Wan et al., 2017). In this study, we use the kaolinite/smectite ratio as a proxy for humidity (Li et al., 2019), as the formation of kaolinite typically correlates with strong chemical weathering under intense hydrolytic conditions, while smectite formation is related to warm climate conditions with strong seasonality (Chamley, 1989). The origin of kaolinite in marine sediments during the early Cenozoic, especially across the PETM, has been argued to result from the erosion of ancient kaolinite-bearing soil sequences in the source regions rather than corresponding to intense contemporaneous chemical weathering (Thiry & Dupuis, 2000). However, at Site U1514, kaolinite contents do not display any particular correlation with $MAR_{siliciclastic}$, that is, a parameter that is generally used to trace physical erosion and/or terrigenous fluxes (Clift et al., 2014), hence ruling out any significant contribution of inherited kaolinite. Besides, increased kaolinite content observed during the high-sea-level early Eocene suggests insignificant influence of differential settling on clay mineral assemblages of Site U1514 (e.g., Handley et al., 2011).

Despite subtle differences, $\Delta\varepsilon_{Hfclay}$, kaolinite/smectite, and Mg/Al clearly collectively suggest limited weathering variability during the mid-late Paleocene, followed by large-scale fluctuations in the early Eocene, punctuated by an abrupt event of intense chemical weathering across the PETM (Figure 2). Instead, the Zr/Rb ratio, an indirect proxy for grain-size and eolian versus fluvial detrital inputs (e.g., Crocker et al., 2022), displays an upward decreasing trend, with high-frequency fluctuations during mid-late Paleocene (Figure 2). The observed Zr/Rb trend is consistent with the median grain size record at Site U1514 (Figure 1), suggesting a gradual shift toward enhanced fluvial inputs during the early Eocene.

During the 62–56 Ma time interval, relatively less humid conditions can be inferred by very low kaolinite/smectite, suggestive of reduced continental surface weathering in SW Australia, as also inferred from the observed low values of $\Delta\varepsilon_{Hfclay}$ and high Mg/Al at Site U1514 (Figure 2b). Interestingly, the low-resolution

$\Delta\varepsilon_{Hfclay}$ data records an additional marked decrease in continental surface silicate weathering at ~59.5 Ma, correlating well with a short-lived cooling event recorded by $TEX_{86}$-derived sea surface temperature (SST) of ODP Site 1,172 off northern Tasmania (Hollis et al., 2014). Given that no obvious correlation was observed between $\varepsilon_{Hf}$, Zr content and $\varepsilon_{Nd}$, any potential influence from a putative "zircon effect" and/or provenance changes is unlikely to account for the observed negative excursion of $\Delta\varepsilon_{Hfclay}$ at Site U1514 (Bayon et al., 2016; Dataset S1). This short-lived event that occurred during the middle/late Paleocene transition has been previously reported elsewhere in central Pacific and south Atlantic Ocean and is known as the Mid-Paleocene Biotic Event (MPBE), which is typically identified by carbonate dissolution and substantial change in microfossil assemblages (Hancock & Dickens, 2006; Petrizzo, 2005). At Site U1514, the presence of this short-lived cooling event is further evidenced by concomitant increases in $MAR_{siliciclastic}$ at ~59.5 Ma (Figure S2 in Supporting Information S1), which is likely the result of greater coastal erosion due to sea-level fall, as also observed in many ODP sites and terrestrial records at similar latitudes (Hollis et al., 2014).

Across the PETM, which represents the most extreme carbon cycle perturbation of the early Cenozoic (Zachos et al., 2003), most records at Site U1514 display considerable changes. Collectively, the changes observed in kaolinite/smectite, Mg/Al, Zr/Rb and $\Delta\varepsilon_{Hfclay}$ indicate an abrupt shift toward wetter climate conditions in SW Australia associated with enhanced chemical weathering and fluvial inputs (Figure 2). Meanwhile, a shift in provenance, suggestive of enhanced sediment contribution from distant catchment regions, is also inferred from elevated LREE/HREE ratio and a negative excursion of $\varepsilon_{Nd}$ (Figure 2; Chen et al., 2022). The observed changes in humidity and drainage reorganization coincide with vegetation proxy records from southern Australia and ODP Site 1,172, which documented rapid expansion of meso-megathermal rain forests at southern high latitudes at the onset of the PETM (Contreras et al., 2014; Huurdeman et al., 2020; Sluijs et al., 2011). During 55–51 Ma, although the detailed correlation between proxy records is unclear, the combination of the kaolinite/smectite, Mg/Al, Zr/Rb ratios and $\Delta\varepsilon_{Hfclay}$ suggest an overall trend toward more humid conditions, coinciding with the long-term early Eocene global warming (Kirtland Turner et al., 2014; Sexton et al., 2011). The concurrent provenance shifts further suggest that enhanced humidity during the early Eocene was accompanied by drainage reorganization in the catchment regions (Figure 2a).

To summarize, during the mid-late Paleocene, mid–high southern latitudes regions in SW Australia experienced a relatively stable climate that gradually shifted toward more humid conditions from the early Eocene, interspersed with abrupt environmental changes across the short-lived cooling and hyperthermal events of MPBE and PETM, respectively.

### 4.3. Implications for the Migration of SH Westerlies

Although the exact position of SH westerlies during the early Cenozoic cannot be constrained by existing proxy data, modeling studies suggest that Australia was dominated by SH westerlies due to its southernmost paleo-geographic location compared to the present (Carmichael et al., 2018; Liu et al., 2017; Reichgelt et al., 2022; Shields et al., 2021). In particular, the SW Australian region, with a paleolatitude of ~55°S, was possibly located at the southern margin of the wind belt; as such, it would have experienced a hydroclimate pattern controlled by the latitudinal migration and strength of the SH westerlies (Reichgelt et al., 2022; Shields et al., 2021). Given that the records of kaolinite/smectite, Zr/Rb, $\Delta\varepsilon_{Hfclay}$ and Mg/Al at Site U1514 were predominantly or at least partially controlled by the humidity (i.e., precipitation change) of SW Australia, those proxies thus can be used to trace the changes in SH westerlies during the early Cenozoic (Figure 2).

During the present-day austral winters, SH westerlies tend to extend northward with decreased wind intensity, while moving southward with strengthened intensity during the austral summer (Lamy et al., 2010). A relatively more distant position of the SH westerlies from SW Australia and/or a weaker atmospheric circulation is suspected from the observed limited variability in precipitation proxy records during the mid-late Paleocene, especially across the MPBE, as inferred from reduced humidity levels, riverine runoff, and continental weathering (Figure 2). Such observation is consistent with the vegetation and paleo-temperature reconstructions from the East Tasman Plateau (paleolatitude: ~65°S) and eastern New Zealand (paleolatitude: ~50–60°S), which indicate a warm-temperate climate during mid-late Paleocene and cool-temperate conditions across mid/late Paleocene transition (~59.5–59.0 Ma) (Contreras et al., 2014; Hollis et al., 2014). Weakened SH westerlies would simply result in a consistent decrease of rainfall/circulation intensity along the mid to high latitudes covered by the wind belt. In contrast to Site U1514, however, terrestrial records from Cerro Bayo in northwestern Argentina

(paleolatitude: ∼35–40°S), which was situated close to the northern margin of the SH westerlies, document a rapid increase in temperature and precipitation across the MPBE (Figure 2d) (Hyland et al., 2015). Furthermore, the eolian dust grain size records from DSDP Site 215 (∼45–50°S), which have been used to track the intensity of SH atmospheric circulation, show a transient increase at ∼59.5 Ma (Figure 2d; Hovan & Rea, 1992). Such discrepancies in the hydroclimate/circulation between Site U1514 and locations further north thus can be only explained by a northward migration of the SH westerlies, which placed the wind belt center (possibly near ∼50°S) further away from SW Australia, especially across the MPBE.

High-precipitation climate thrived at mid–high latitudes starting from the early Eocene, especially across the PETM, as indicated by increased humidity in SW Australia (this study), Margaret Point in southeast Australia (Huurdeman et al., 2020), Tasmania (Contreras et al., 2014), and New Zealand (Sluijs et al., 2011). The globally elevated temperatures during the early Eocene likely contributed to a "supercharged" hydrological cycle, via increased water vapor being transported from the tropics to high latitudes (Carmichael et al., 2017; Reichgelt et al., 2022; Shields et al., 2021). However, in addition to a more active hydrological cycle owing to greenhouse climate conditions, enhanced moisture from the incoming westerlies must have exerted additional influence, as supported by a relatively higher modeled Eocene precipitation of SW Australia compared to the interior lands in Eastern Australia (Reichgelt et al., 2022). In particular, across the PETM, a reduction in the intensity of SH atmospheric circulation has been inferred from decreased eolian grain sizes at DSDP Site 215 (∼45°–50°S) (Figure 2d) (Hovan & Rea, 1992), thus suggesting a southward displacement of the SH westerlies under short-lived hyperthermal conditions (Figure 2). By analogy, despite the lack of any available supporting evidence from dust accumulation record for southernmost latitudes in the early Eocene, we infer a further south location of the SH westerlies' center (possibly close to ∼60°S) during the early Eocene (Figure 2). This would thus result in more humid conditions prevailing at southern high latitudes compared to the mid-late Paleocene interval.

### 4.4. Possible Mechanisms Driving the Migration of SH Westerlies During the Early Cenozoic

Over geological timescales, changes in the position and intensity of the westerlies have been suggested to be predominately regulated by equator-to-pole temperature gradients and/or the extent of the ice sheet (Abell et al., 2021; Goyal et al., 2021; Groeneveld et al., 2017; Lamy et al., 2010). Additionally, tectonic forcing such as topographic uplift and continental drift might also change the course of the westerlies or the relative landfall position of the associated rain belt (Liu et al., 2017; Tang et al., 2022). Nevertheless, the significant northward motion of the Australian plate was not initiated until the mid-Eocene (∼45 Ma) (Hall, 2012; Li & Powell, 2001; Wang et al., 2022). Moreover, one would expect a gradual increase in humidity if tectonic forcing (i.e., northward drifting) had played a major role in accounting for our proxy records, which is obviously inconsistent with the large variability observed for for example, kaolinite at Site U1514 during the early Eocene (Figure 2; Wang et al., 2022). Therefore, we infer that the hydroclimate evolution of SW Australia cannot be explained by tectonic forcing alone, suggesting additional climatic controls.

During the mid–late Paleocene, Mg/Ca ratio records from ODP Site 865 (paleolatitude: ∼2°N) in the central equatorial Pacific Ocean indicate relatively high and stable tropical SST (Tripati et al., 2003). At the same time, a warm temperate climate prevailed at southern high latitudes except for a short-lived cooling event at ∼59.5 Ma, thus resulting in no, or only minor, changes to latitudinal SST gradients throughout much of this interval (Contreras et al., 2014; Hollis et al., 2012). We infer this relatively stable climate setting largely explains the limited variability of our precipitation proxy records for SW Australia during mid-late Paleocene. Conversely, a markedly decreased latitudinal SST gradient between sub-equator and sub-polar was observed during the early Eocene (∼55–51 Ma), as evidenced by much warmer mid–high latitudes and slightly warmer low latitudes (Figure 2e) (Bijl et al., 2009; Gaskell et al., 2022). Additionally, exceptional low meridional temperature gradients have been reported across the PETM, in response to the extreme global warmth related to elevated $CO_2$ levels (Gaskell et al., 2022). This pattern would potentially contribute to a poleward shift of the SH westerlies, thus transporting increased moisture to mid–high latitudes, especially across the PETM (Figure 2). The consistency among $TEX_{86}$-derived SST at ODP Site 1,172 and precipitation-related proxies at Site U1514 adds further support for major climate control over SH westerlies (Bijl et al., 2009, 2013; Hollis et al., 2014). High-latitude surface temperatures are particularly sensitive to global climate change and are thus likely to dominate the evolution of latitudinal SST gradients over geological timescales, especially under greenhouse conditions.

At the mid/late Paleocene transition (∼59.5 Ma), short-lived cooling associated with the MPBE has been inferred from various terrestrial and marine records at southern high latitudes (Hollis et al., 2012, 2014). This cooling event could relate to the growth of ephemeral ice sheets in upland regions of Antarctica, possibly resulting from atmospheric $CO_2$ drawdown (Hollis et al., 2014). Though disputed, a recent study has indeed proposed that mountain glaciers were likely present in the Transantarctic Mountains of Antarctica during the mid-late Paleocene (∼60–56 Ma) (Barr et al., 2022), which would have potentially resulted in a greater atmospheric pressure difference between low- and high-latitudes and, as a consequence, in the northward migration of the SH westerlies. Such a SH atmospheric circulation shift would have moved the core of the rain belt away from SW Australia, thus explaining the differentiated hydroclimate conditions observed across the mid–high latitudinal band (Figure 2).

As discussed above, our proxy records suggest that the hydroclimate evolution of mid–high latitudes during the early Cenozoic was dominated by the latitudinal migration of SH westerlies, probably driven by equator-to-pole temperature gradients. Of course, our reconstruction is based on one single case study and as such it can only provide limited constraints on the exact extent of the meridional SH westerlies shift at that time. Additional studies will be needed to reconstruct the large-scale evolution of the SH westerlies based on multiple records along a wider latitudinal band or on a global view. Nevertheless, given that the early Cenozoic is considered one of the closest analogs for future climate change (e.g., Norris et al., 2013), our findings still provide direct support that current anthropogenic warming could result in a poleward migration of the present-day westerlies. The resulting reorganization of SH atmospheric circulation pattern would also likely affect the global carbon cycle, via its presumed impact on regional upwelling and marine productivity.

## 5. Concluding Remarks

IODP Site U1514 in the Mentelle Basin (Southeastern Indian Ocean) provides an excellent record of early Cenozoic paleoclimate evolution at mid–high southern latitudes influenced by the westerlies. Our multi-proxy investigation for the 62–51 Ma time interval indicates that detrital sediments deposited at Site U1514 were mainly derived from the Leeuwin Block and the Perth Basin in SW Australia, with additional contributions from more distant catchment regions (i.e., Yilgarn Craton) since the early Eocene. Various precipitation-related proxies suggest less humid and relatively stable climate conditions during the mid–late Paleocene (62–56 Ma), followed by a gradual increase in humidity since the early Eocene (55–51 Ma). This long-term hydroclimate pattern was punctuated by abrupt decreases and increases in humidity at ∼59.5 Ma and ∼55.9 Ma, corresponding to the short-lived cooling (MPBE) and hyperthermal (PETM) events, respectively.

We argue that the latitudinal migration of the SH westerlies controlled by changes in the equator-to-pole temperature gradient drove the variability of precipitation proxy records at Site U1514. Though the potential influence of tectonic forcing (i.e., northward continental drifting) cannot be fully excluded, we propose that the SH westerlies remain relatively stable during the mid-late Paleocene, before shifting southward from the early Eocene, largely caused by markedly reduced latitudinal temperature gradients under greenhouse warming conditions, especially across the PETM. The presence of ephemeral ice sheets in highlands of Antarctica during the mid-late Paleocene most likely forced a transient northward migration of the SH westerlies during the MPBE. Our study emphasizes the significant role the SH westerlies on hydroclimate conditions at mid–high latitudes during the early Cenozoic. By analogy, and in agreement with previous reconstructions for the late Cenozoic, our findings provide further evidence that the current global warming could progressively result in the poleward migration of the westerlies.

## Data Availability Statement

The original data present in this study are included in the in Supporting Information S1. Supplementary data are archived in an open-source online data repository hosted at the Zenodo database via Chen and Xu (2024).

## References

Abell, J. T., Winckler, G., Anderson, R. F., & Herbert, T. D. (2021). Poleward and weakened westerlies during Pliocene warmth. *Nature*, *589*(7840), 70–75. https://doi.org/10.1038/s41586-020-03062-1

Barr, I. D., Spagnolo, M., Rea, B. R., Bingham, R. G., Oien, R. P., Adamson, K., et al. (2022). 60 million years of glaciation in the transantarctic mountains. *Nature Communications*, *13*(1), 5526. https://doi.org/10.1038/s41467-022-33310-z

Bayon, G., Bindeman, I. N., Trinquier, A., Retallack, G. J., & Bekker, A. (2022). Long-term evolution of terrestrial weathering and its link to Earth's oxygenation. *Earth and Planetary Science Letters*, *584*, 117490. https://doi.org/10.1016/j.epsl.2022.117490

Bayon, G., Skonieczny, C., Delvigne, C., Toucanne, S., Bermell, S., Ponzevera, E., & André, L. (2016). Environmental Hf–Nd isotopic decoupling in World river clays. *Earth and Planetary Science Letters*, *438*, 25–36. https://doi.org/10.1016/j.epsl.2016.01.010

Bayon, G., Toucanne, S., Skonieczny, C., André, L., Bermell, S., Cheron, S., et al. (2015). Rare earth elements and neodymium isotopes in world river sediments revisited. *Geochimica et Cosmochimica Acta*, *170*, 17–38. https://doi.org/10.1016/j.gca.2015.08.001

Beard, J. S. (1999). Evolution of the river systems of the south-west drainage division, Western Australia. *Journal of the Royal Society of Western Australia*, *82*, 147–164.

Bijl, P. K., Schouten, S., Sluijs, A., Reichart, G. J., Zachos, J. C., & Brinkhuis, H. (2009). Early palaeogene temperature evolution of the southwest Pacific Ocean. *Nature*, *461*(7265), 776–779. https://doi.org/10.1038/nature08399

Bijl, P. K., Sluijs, A., & Brinkhuis, H. (2013). A magneto- and chemostratigraphically calibrated dinoflagellate cyst zonation of the early Palaeogene South Pacific Ocean. *Earth-Science Reviews*, *124*, 1–31. https://doi.org/10.1016/j.earscirev.2013.04.010

Borissova, I., Bradshaw, B., Nicholson, C., Struckmeyer, H., & Payne, D. (2010). New exploration opportunities on the southwest Australian margin—Deep-water frontier Mentelle Basin. *The APPEA Journal*, *50*(1), 47–60. https://doi.org/10.1071/aj09004

Carmichael, M. J., Inglis, G. N., Badger, M. P. S., Naafs, B. D. A., Behrooz, L., Remmelzwaal, S., et al. (2017). Hydrological and associated biogeochemical consequences of rapid global warming during the Paleocene-Eocene Thermal Maximum. *Global and Planetary Change*, *157*, 114–138. https://doi.org/10.1016/j.gloplacha.2017.07.014

Carmichael, M. J., Pancost, R. D., & Lunt, D. J. (2018). Changes in the occurrence of extreme precipitation events at the Paleocene–Eocene thermal maximum. *Earth and Planetary Science Letters*, *501*, 24–36. https://doi.org/10.1016/j.epsl.2018.08.005

Chamley, H. (1989). *Clay sedimentology*. Springer.

Chen, H., Bayon, G., Xu, Z., & Li, T. (2023). Hafnium isotope evidence for enhanced weatherability at high southern latitudes during Oceanic Anoxic Event 2. *Earth and Planetary Science Letters*, *601*, 117910. https://doi.org/10.1016/j.epsl.2022.117910

Chen, H., & Xu, Z. (2024). Supplementary material from: Meridional shifts of the southern Hemisphere westerlies during the early Cenozoic [Dataset]. *Zenodo*. https://doi.org/10.5281/zenodo.12159313

Chen, H., Xu, Z., Bayon, G., Lim, D., Batenburg, S. J., Petrizzo, M. R., et al. (2022). Enhanced hydrological cycle during Oceanic Anoxic Event 2 at southern high latitudes: New insights from IODP Site U1516. *Global and Planetary Change*, *209*, 103735. https://doi.org/10.1016/j.gloplacha.2022.103735

Clift, P. D., Wan, S. M., & Blusztajn, J. (2014). Reconstructing chemical weathering, physical erosion and monsoon intensity since 25 Ma in the northern South China Sea: A review of competing proxies. *Earth-Science Reviews*, *130*, 86–102. https://doi.org/10.1016/j.earscirev.2014.01.002

Contreras, L., Pross, J., Bijl, P. K., O'Hara, R. B., Raine, J. I., Sluijs, A., & Brinkhuis, H. (2014). Southern high-latitude terrestrial climate change during the Palaeocene–Eocene derived from a marine pollen record (ODP Site 1172, East Tasman Plateau). *Climate of the Past*, *10*(4), 1401–1420. https://doi.org/10.5194/cp-10-1401-2014

Corentin, P., Pucéat, E., Pellenard, P., Freslon, N., Guiraud, M., Blondet, J., et al. (2022). Hafnium-neodymium isotope evidence for enhanced weathering and uplift-climate interactions during the Late Cretaceous. *Chemical Geology*, *591*, 120724. https://doi.org/10.1016/j.chemgeo.2022.120724

Crame, J. A. (2020). Early Cenozoic evolution of the latitudinal diversity gradient. *Earth-Science Reviews*, *202*, 103090. https://doi.org/10.1016/j.earscirev.2020.103090

Crocker, A. J., Naafs, B. D. A., Westerhold, T., James, R. H., Cooper, M. J., Röhl, U., et al. (2022). Astronomically controlled aridity in the Sahara since at least 11 million years ago. *Nature Geoscience*, *15*(8), 671–676. https://doi.org/10.1038/s41561-022-00990-7

Deconto, R. M., & Pollard, D. (2003). Rapid Cenozoic glaciation of Antarctica induced by declining atmospheric $CO_2$. *Nature*, *421*(6920), 245–249. https://doi.org/10.1038/nature01290

Edgar, K. M., MacLeod, K. G., Hasegawa, T., Hanson, E. M., Boomer, I., & Kirby, N. (2022). Data report: Cenozoic and Upper Cretaceous bulk carbonate stable carbon and oxygen isotopes from IODP Expedition 369 Sites U1513, U1514, and U1516 in the southeast Indian Ocean. *Proceedings of the International Ocean Discovery Program*, *369*(206). https://doi.org/10.14379/iodp.proc.369.206.2022

Fan, Q., Xu, Z., MacLeod, K. G., Brumsack, H. J., Li, T., Chang, F., et al. (2022). First record of oceanic anoxic event 1d at southern high latitudes: Sedimentary and geochemical evidence from International Ocean Discovery Program expedition 369. *Geophysical Research Letters*, *49*(10), e2021GL097641. https://doi.org/10.1029/2021gl097641

Gaskell, D. E., Huber, M., O'Brien, C. L., Inglis, G. N., Acosta, R. P., Poulsen, C. J., & Hull, P. M. (2022). The latitudinal temperature gradient and its climate dependence as inferred from foraminiferal $\delta^{18}O$ over the past 95 million years. *Proceedings of the National Academy of Sciences*, *119*(11), e2111332119. https://doi.org/10.1073/pnas.2111332119

Goyal, R., Sen Gupta, A., Jucker, M., & England, M. H. (2021). Historical and projected changes in the southern Hemisphere surface westerlies. *Geophysical Research Letters*, *48*(4), e2020GL090849. https://doi.org/10.1029/2020gl090849

Groeneveld, J., Henderiks, J., Renema, W., McHugh, C. M., De Vleeschouwer, D., Christensen, B. A., et al. (2017). Australian shelf sediments reveal shifts in Miocene Southern Hemisphere westerlies. *Science Advances*, *3*(5), e1602567. https://doi.org/10.1126/sciadv.1602567

Hall, R. (2012). Late Jurassic-Cenozoic reconstructions of the Indonesian region and the Indian Ocean. *Tectonophysics*, *570–571*, 1–41. https://doi.org/10.1016/j.tecto.2012.04.021

Hancock, H. J. L., & Dickens, G. R. (2006). Carbonate dissolution episodes in Paleocene and Eocene sediment, Shatsky Rise, west-central Pacific. In *Proceedings of the ocean drilling Program Scientific results* (Vol. 198, pp. 1–24). Texas A&M University.

Handley, L., Crouch, E. M., & Pancost, R. D. (2011). A New Zealand record of sea level rise and environmental change during the Paleocene–Eocene Thermal Maximum. *Palaeogeography, Palaeoclimatology, Palaeoecology*, *305*(1–4), 185–200. https://doi.org/10.1016/j.palaeo.2011.03.001

Hodgson, D. A., & Sime, L. C. (2010). Southern westerlies and $CO_2$. *Nature Geoscience*, *3*(10), 666–667. https://doi.org/10.1038/ngeo970

Hollis, C. J., Tayler, M. J. S., Andrew, B., Taylor, K. W., Lurcock, P., Bijl, P. K., et al. (2014). Organic-rich sedimentation in the South Pacific Ocean associated with late Paleocene climatic cooling. *Earth-Science Reviews*, *134*, 81–97. https://doi.org/10.1016/j.earscirev.2014.03.006

Hollis, C. J., Taylor, K. W. R., Handley, L., Pancost, R. D., Huber, M., Creech, J. B., et al. (2012). Early Paleogene temperature history of the southwest Pacific Ocean: Reconciling proxies and models. *Earth and Planetary Science Letters*, *349–350*, 53–66. https://doi.org/10.1016/j.epsl.2012.06.024

Hovan, S. A., & Rea, D. K. (1992). Paleocene/Eocene boundary changes in atmospheric and oceanic circulation: A southern Hemisphere record. *Geology*, *20*(1), 15–18. https://doi.org/10.1130/0091-7613(1992)020<0015:PEBCIA>2.3.CO;2

Huber, B. T., Hobbs, R. W., Bogus, K. A., Batenburg, S. J., Brumsack, H. J., do Monte Guerra, R., et al. (2019). Expedition 369 summary. *Proceedings of the International Ocean Discovery Program*, *369*. https://doi.org/10.14379/iodp.proc.369.101.2019

Huurdeman, E. P., Frieling, J., Reichgelt, T., Bijl, P. K., Bohaty, S. M., Holdgate, G. R., et al. (2020). Rapid expansion of meso-megathermal rain forests into the southern high latitudes at the onset of the Paleocene-Eocene Thermal Maximum. *Geology*, *49*(1), 40–44. https://doi.org/10.1130/g47343.1

Hyland, E. G., Sheldon, N. D., & Cotton, J. M. (2015). Terrestrial evidence for a two-stage mid-Paleocene biotic event. *Palaeogeography, Palaeoclimatology, Palaeoecology*, *417*, 371–378. https://doi.org/10.1016/j.palaeo.2014.09.031

Kirtland Turner, S., Sexton, P. F., Charles, C. D., & Norris, R. D. (2014). Persistence of carbon release events through the peak of early Eocene global warmth. *Nature Geoscience*, *7*(10), 748–751. https://doi.org/10.1038/ngeo2240

Kohn, B. P., Gleadow, A. J. W., Brown, R. W., Gallagher, K., O'sullivan, P. B., & Foster, D. A. (2002). Shaping the Australian crust over the last 300 million years: Insights from fission track thermotectonic imaging and denudation studies of key terranes. *Australian Journal of Earth Sciences*, *49*(4), 697–717. https://doi.org/10.1046/j.1440-0952.2002.00942.x

Komar, N., Zeebe, R. E., & Dickens, G. R. (2013). Understanding long-term carbon cycle trends: The late Paleocene through the early Eocene. *Paleoceanography*, *28*(4), 650–662. https://doi.org/10.1002/palo.20060

Lamy, F., Kilian, R., Arz, H. W., Francois, J.-P., Kaiser, J., Prange, M., & Steinke, T. (2010). Holocene changes in the position and intensity of the southern westerly wind belt. *Nature Geoscience*, *3*(10), 695–699. https://doi.org/10.1038/ngeo959

Lee, E. Y., Wolfgring, E., Tejada, M. L. G., Harry, D. L., Wainman, C. C., Chun, S. S., et al. (2020). Early Cretaceous subsidence of the Naturaliste Plateau defined by a new record of volcaniclastic-rich sequence at IODP Site U1513. *Gondwana Research*, *82*, 1–11. https://doi.org/10.1016/j.gr.2019.12.007

Li, Y., Clift, P. D., Murray, R. W., Exnicios, E., Ireland, T., & Böning, P. (2019). Asian summer monsoon influence on chemical weathering and sediment provenance determined by clay mineral analysis from the Indus Submarine Canyon. *Quaternary Research*, *93*, 23–39. https://doi.org/10.1017/qua.2019.44

Li, Z. X., & Powell, C. M. (2001). An outline of the palaeogeographic evolution of the Australasian region since the beginning of the Neo-proterozoic. *Earth-Science Reviews*, *53*(3–4), 237–277. https://doi.org/10.1016/S0012-8252(00)00021-0

Liu, X., Dong, B., Yin, Z.-Y., Smith, R. S., & Guo, Q. (2017). Continental drift and plateau uplift control origination and evolution of Asian and Australian monsoons. *Scientific Reports*, *7*(1), 40344. https://doi.org/10.1038/srep40344

Maloney, D., Sargent, C., Direen, N. G., Hobbs, R. W., & Gröcke, D. R. (2011). Re-Evaluation of the Mentelle Basin, a polyphase rifted margin basin, offshore south-west Australia: New insights from integrated regional seismic datasets. *Solid Earth Discussions*, *3*(1), 65–103. https://doi.org/10.5194/sed-3-65-2011

Maritati, A., Halpin, J. A., Whittaker, J. M., Daczko, N. R., & Wainman, C. C. (2021). Provenance of Upper Jurassic–lower Cretaceous strata in the Mentelle Basin, southwestern Australia, reveals a trans-Gondwanan fluvial pathway. *Gondwana Research*, *93*, 128–141. https://doi.org/10.1016/j.gr.2020.12.032

Menviel, L., Spence, P., Yu, J., Chamberlain, M. A., Matear, R. J., Meissner, K. J., & England, M. H. (2018). Southern Hemisphere westerlies as a driver of the early deglacial atmospheric $CO_2$ rise. *Nature Communications*, *9*(1), 2503. https://doi.org/10.1038/s41467-018-04876-4

Norris, R. D., Turner, S. K., Hull, P. M., & Ridgwell, A. (2013). Marine ecosystem responses to Cenozoic global change. *Science*, *341*(6145), 492–498. https://doi.org/10.1126/science.1240543

Osei, K. P., Kirkland, C. L., & Mole, D. R. (2021). Nd and Hf isoscapes of the Yilgarn Craton, Western Australia and implications for its mineral systems. *Gondwana Research*, *92*, 253–265. https://doi.org/10.1016/j.gr.2020.12.027

Pearson, P. N., & Palmer, M. R. (2000). Atmospheric carbon dioxide concentrations over the past 60 million years. *Nature*, *406*(17), 695–699. https://doi.org/10.1038/35021000

Petrizzo, M. R. (2005). An early late Paleocene event on Shatsky rise, northwest Pacific Ocean (ODP Leg 198): Evidence from planktonic foraminiferal assemblages. In *Proceedings of the ocean drilling program* (Vol. 198). Ocean Drilling Program.

Pourmand, A., Dauphas, N., & Ireland, T. J. (2012). A novel extraction chromatography and MC-ICP-MS technique for rapid analysis of REE, Sc and Y: Revising CI-chondrite and Post-Archean Australian Shale (PAAS) abundances. *Chemical Geology*, *291*, 38–54. https://doi.org/10.1016/j.chemgeo.2011.08.011

Reichgelt, T., Greenwood, D. R., Steinig, S., Conran, J. G., Hutchinson, D. K., Lunt, D. J., et al. (2022). Plant proxy evidence for high rainfall and productivity in the Eocene of Australia. *Paleoceanography and Paleoclimatology*, *37*(6), e2022PA004418. https://doi.org/10.1029/2022pa004418

Saunders, K. M., Kamenik, C., Hodgson, D. A., Hunziker, S., Siffert, L., Fischer, D., et al. (2012). Late Holocene changes in precipitation in northwest Tasmania and their potential links to shifts in the Southern Hemisphere westerly winds. *Global and Planetary Change*, *92–93*, 82–91. https://doi.org/10.1016/j.gloplacha.2012.04.005

Sexton, P. F., Norris, R. D., Wilson, P. A., Palike, H., Westerhold, T., Rohl, U., et al. (2011). Eocene global warming events driven by ventilation of oceanic dissolved organic carbon. *Nature*, *471*(7338), 349–352. https://doi.org/10.1038/nature09826

Shields, C. A., Kiehl, J. T., Rush, W., Rothstein, M., & Snyder, M. A. (2021). Atmospheric rivers in high-resolution simulations of the Paleocene Eocene Thermal Maximum (PETM). *Palaeogeography, Palaeoclimatology, Palaeoecology*, *567*, 110293. https://doi.org/10.1016/j.palaeo.2021.110293

Shulmeister, J., Goodwin, I., Renwick, J., Harle, K., Armand, L., McGlone, M. S., et al. (2004). The southern Hemisphere westerlies in the Australasian sector over the last glacial cycle: A synthesis. *Quaternary International*, *118–119*, 23–53. https://doi.org/10.1016/s1040-6182(03)00129-0

Sluijs, A., Bijl, P. K., Schouten, S., Röhl, U., Reichart, G. J., & Brinkhuis, H. (2011). Southern ocean warming, sea level and hydrological change during the Paleocene-Eocene thermal maximum. *Climate of the Past*, *7*(1), 47–61. https://doi.org/10.5194/cp-7-47-2011

Sun, T., Xu, Z., Chang, F., & Li, T. (2022). Climate evolution of southwest Australia in the Miocene and its main controlling factors. *Science China Earth Sciences*, *65*(6), 1104–1115. https://doi.org/10.1007/s11430-021-9904-y

Sykes, T. J. S., & Kidd, R. B. (1994). Volcanogenic sediment distributions in the Indian Ocean through the Cretaceous and Cenozoic, and their paleoenvironmental implications. *Marine Geology*, *116*(3–4), 267–291. https://doi.org/10.1016/0025-3227(94)90046-9

Tang, Y., Wan, S., Clift, P. D., Zhao, D., Xu, Z., Zhang, J., et al. (2022). Northward shift of the Northern Hemisphere westerlies in the early to late Miocene and its links to Tibetan uplift. *Geophysical Research Letters*, *49*(18), e2022GL099311. https://doi.org/10.1029/2022gl099311

Thiry, M., & Dupuis, C. (2000). Use of clay minerals for paleoclimatic reconstructions: Limits of the method with special reference to the Paleocene—Lower Eocene interval. *Gff*, *122*(1), 166–167. https://doi.org/10.1080/11035890001221166

Thomas, E., Brinkhuis, H., Huber, M., & Rohl, U. (2006). An Ocean view of the early Cenozoic greenhouse world. *Oceanography*, *19*(4), 94–103. https://doi.org/10.5670/oceanog.2006.08

Tripati, A. K., Delaney, M. L., Zachos, J. C., Anderson, L. D., Kelly, D. C., & Elderfield, H. (2003). Tropical sea-surface temperature reconstruction for the early Paleogene using Mg/Ca ratios of planktonic foraminifera. *Paleoceanography*, *18*(4), 1101. https://doi.org/10.1029/2003pa000937

Vahlenkamp, M., De Vleeschouwer, D., Batenburg, S. J., Edgar, K. M., Hanson, E., Martinez, M., et al. (2020). A lower to middle Eocene astrochronology for the Mentelle Basin (Australia) and its implications for the geologic time scale. *Earth and Planetary Science Letters*, *529*, 115865. https://doi.org/10.1016/j.epsl.2019.115865

Wan, S., Clift, P. D., Zhao, D., Hovius, N., Munhoven, G., France-Lanord, C., et al. (2017). Enhanced silicate weathering of tropical shelf sediments exposed during glacial lowstands: A sink for atmospheric CO2. *Geochimica et Cosmochimica Acta*, *200*, 123–144. https://doi.org/10.1016/j.gca.2016.12.010

Wang, W., Colin, C., Xu, Z., Lim, D., Wan, S., & Li, T. (2022). Tectonic and climatic controls on sediment transport to the southeast Indian Ocean during the Eocene: New insights from IODP site U1514. *Global and Planetary Change*, *217*, 103956. https://doi.org/10.1016/j.gloplacha.2022.103956

Westerhold, T., Marwan, N., Drury, A. J., Liebrand, D., Agnini, C., Anagnostou, E., et al. (2020). An astronomically dated record of Earth's climate and its predictability over the last 66 million years. *Science*, *369*(6509), 1383–1387. https://doi.org/10.1126/science.aba6853

White, L. T., Forster, M. A., Tanner, D., Tejada, M. L. G., Hobbs, R., & Party, I. E. S. (2022). Age of magmatism and alteration of basaltic rocks cored at the base of IODP Site U1513 Naturaliste Plateau, southwestern Australia. *Australian Journal of Earth Sciences*, *69*(3), 383–405. https://doi.org/10.1080/08120099.2021.1963840

Wilde, S. A., & Nelson, D. R. (2001). *Record 2001/15: Geology of the western yigarn Craton and Leeuwin complex, western Australia—a field guide*. Geological Survey.

Zachos, J., Pagani, M., Sloan, L., Thomas, E., & Billups, K. (2001). Trends, rhythms, and aberrations in global climate 65 Ma to present. *Science*, *292*(5517), 686–693. https://doi.org/10.1126/science.1059412

Zachos, J. C., Dickens, G. R., & Zeebe, R. E. (2008). An early Cenozoic perspective on greenhouse warming and carbon-cycle dynamics. *Nature*, *451*(7176), 279–283. https://doi.org/10.1038/nature06588

Zachos, J. C., Wara, M. W., Bohaty, S., Delaney, M. L., Petrizzo, M. R., Brill, A., et al. (2003). A transient rise in tropical sea surface temperature during the Paleocene-Eocene thermal maximum. *Science*, *302*(5650), 1551–1554. https://doi.org/10.1126/science.1090110

## References From the Supporting Information

Bayon, G., German, C. R., Boella, R. M., Milton, J. A., Taylor, R. N., & Nesbitt, R. W. (2002). An improved method for extracting marine sediment fractions and its application to Sr and Nd isotopic analysis. *Chemical Geology*, *187*(3–4), 179–199. https://doi.org/10.1016/S0009-2541(01)00416-8

Biscaye, P. E. (1965). Mineralogy and sedimentation of recent deep-sea clay in the Atlantic Ocean and adjacent seas and oceans. *Geological Society of America Bulletin*, *76*(7), 803–832. https://doi.org/10.1130/0016-7606(1965)76[803:MASORD]2.0.CO;2

Bouvier, A., Vervoort, J. D., & Patchett, P. J. (2008). The Lu–Hf and Sm–Nd isotopic composition of CHUR: Constraints from unequilibrated chondrites and implications for the bulk composition of terrestrial planets. *Earth and Planetary Science Letters*, *273*(1–2), 48–57. https://doi.org/10.1016/j.epsl.2008.06.010

Chu, N.-C., Taylor, R. N., Chavagnac, V., Nesbitt, R. W., Boella, R. M., Milton, J. A., et al. (2002). Hafnium isotope ratio analysis using multi-collector inductively coupled plasma mass spectrometry: An evaluation of isobaric interference corrections. *Journal of Analytical Atomic Spectrometry*, *17*(12), 1567–1574. https://doi.org/10.1039/b206707b

Rea, D. K., & Janecek, T. R. (1981). Late cretaceous history of eolian deposition in the mid-pacific mountains, central North Pacific Ocean. *Palaeogeography, Palaeoclimatology, Palaeoecology*, *36*(1–2), 55–67. https://doi.org/10.1016/0031-0182(81)90048-1

Vervoort, J. D., Plank, T., & Prytulak, J. (2011). The Hf–Nd isotopic composition of marine sediments. *Geochimica et Cosmochimica Acta*, *75*(20), 5903–5926. https://doi.org/10.1016/j.gca.2011.07.046